RIACS

Research Institute for Advanced Computer Science
NASA Ames Research Center

An Overset Grid Navier-Stokes/Kirchhoff-Surface Method for Rotorcraft Aeroacoustic Predictions

Earl P. N. Duque
Roger C. Strawn
Jasim Ahmad
Rupak Biswas

RIACS Technical Report 96.06 February 1996

Paper No. AIAA-96-0152, presented at the *AIAA 34th Aerospace Sciences Meeting & Exhibit*, Reno, Nevada, January 15–18, 1996

An Overset Grid Navier-Stokes/Kirchhoff-Surface Method for Rotorcraft Aeroacoustic Predictions

Earl P. N. Duque
Roger C. Strawn
Jasim Ahmad
Rupak Biswas

The Research Institute of Advanced Computer Science is operated by Universities Space Research Association, The American City Building, Suite 212, Columbia, MD 21044, (410) 730-2656

Work reported herein was supported by NASA via Contract NAS 2-13721 between NASA and the Universities Space Research Association (USRA). Work was performed at the Research Institute for Advanced Computer Science (RIACS), NASA Ames Research Center, Moffett Field, CA 94035-1000.

AN OVERSET GRID NAVIER-STOKES/KIRCHHOFF- SURFACE METHOD FOR ROTORCRAFT AEROACOUSTIC PREDICTIONS

Earl P. N. Duque & Roger C. Strawn
US Army Aeroflightdynamics Directorate, ATCOM, Ames Research Center, Moffett Field, CA

Jasim Ahmad
Sterling Software, NASA Ames Research Center, Moffett Field, CA
and
Rupak Biswas
RIACS, NASA Ames Research Center, Moffett Field, CA

Abstract

This paper describes a new method for computing the flowfield and acoustic signature of arbitrary rotors in forward flight. The overall scheme uses a finite-difference Navier-Stokes solver to compute the aerodynamic flowfield near the rotor blades. The equations are solved on a system of overset grids that allow for prescribed cyclic and flapping blade motions and capture the interactions between the rotor blades and wake. The far-field noise is computed with a Kirchhoff integration over a surface that completely encloses the rotor blades. Flowfield data are interpolated onto this Kirchhoff surface using the same overset-grid techniques that are used for the flowfield solution. As a demonstration of the overall prediction scheme, computed results for far-field noise are compared with experimental data for both high-speed impulsive (HSI) and blade-vortex interaction (BVI) cases. The HSI case showed good agreement with experimental data while a preliminary attempt at the BVI case did not. The computations clearly show that temporal accuracy, spatial accuracy and grid resolution in the Navier-Stokes solver play key roles in the overall accuracy of the predicted noise. These findings will be addressed more closely in future BVI computations. Overall, the overset-grid CFD scheme provides a powerful new framework for the prediction of helicopter noise

Introduction

Modern helicopter designs aim for low noise and this is particularly true for civilian helicopters that operate near heavily populated areas. There are two main types of noise that cause problems for helicopters. The first is called high-speed impulsive (HSI) noise and consists of a strong acoustic disturbance occurring over a short period of time. Impulsive noise is generally associated with high tip speeds and advancing-tip Mach numbers greater than 0.9. The second type of noise comes from the interaction of the rotor blades with their vortical wake systems. This type of noise is called blade-vortex interaction (BVI) noise and it is particularly important when the helicopter is descending for landings.

Accurate prediction of both types of rotor noise is heavily dependent on the accurate prediction of the aerodynamic flowfield around the rotor blades. Tip vortices in the rotor wakes dominate the flowfield and produce a highly unsteady and nonuniform induced velocity field at the rotor disk. These rotor wakes are very difficult to model but they hold the key to accurate acoustic predictions.

Flowfield models based on computational fluid dynamics (CFD) hold a great deal of promise for simulating the aerodynamics of helicopter rotors and their wake systems. The rotor wakes can be captured directly without ad-hoc models and the nonlinear flowfield close to the rotor blades is modeled accurately. Overset grid schemes allow for efficient grids around complicated geometries and also provide a framework for solution adaption and better resolution of the wake system.

The CFD solutions in this paper use the overset grid method for helicopter aerodynamics that was developed by Ahmad and Duque[1]. The method includes a user-prescribed motion of the blade that models the effects of cyclic pitch control and the rotor blade flapping. The interactions between the rotor blades and their wake systems are captured as an integral part of the CFD solution. References [2-4] provide additional examples

Presented at the 34th Aerospace Sciences Meeting & Exhibit, Reno, NV, January 15-18, 1996.

of overset-grid CFD methods for helicopter aerodynamics.

Even if the flowfield near the rotor blade is computed accurately with a CFD model, it is not practical to extend this CFD solution to compute the helicopter acoustics in the far field. Away from the rotor blades, more efficient Kirchhoff methods for acoustic propagation can be used that are based on linear theory. This type of combined solution method is a good compromise between efficiency and accuracy. The CFD equations model the nonlinear effects near the rotor blade surfaces and the linear Kirchhoff methods propagate the acoustic signal to the far field in a computationally-efficient manner.

The Kirchhoff method computes the acoustic pressure in the far field from a numerical integration over a surface that completely encloses the rotor blades. Aerodynamic and acoustic solutions in the near field are computed with an appropriate CFD method and interpolated onto the Kirchhoff surface using overset-grid interpolation tools and then stored for acoustic postprocessing. The Kirchhoff acoustics prediction scheme from Strawn et al. [5,6] is used in this paper. It is specifically developed for compatibility with overset grid systems and previous results with this scheme have compared very well with experimental data for both HSI and BVI noise.

The combination of CFD solutions near the rotor blade with Kirchhoff methods for the far-field offers high accuracy with reasonable computer resource requirements. By incorporating the Kirchhoff surface into the existing framework for overset-grid CFD solvers, we can compute the far-field acoustics solution with very little additional cost compared to the CFD solution alone.

This main purpose of this paper is to present the framework for our new combined aeroacoustics prediction method. Computed results for HSI and BVI noise are preliminary at present and will improve as we fine-tune individual parts of the overall scheme.

CFD Methodology

Algorithm

The main flowsolver is based upon the OVERFLOW1.6ap code by Buning [7]. OVERFLOW 1.6ap is a general purpose Navier-Stokes code for static grid type computations. Meakin [3] used an earlier version of the OVERFLOW code and coupled his domain connectivity algorithm (DCF) to the solver. Ahmad and Duque [1] used the same connectivity algorithm but coupled it to another flowsolver and included the capability for arbitrary rigid blade motion. In our current work, the generality of the OVERFLOW code is combined with the dynamic grid capability of DCF and arbitrary rigid blade motion.

The OVERFLOW code has a number of available flow solvers such as the block Beam-Warming scheme. However, stability constraints severely limit the timestep requirements. Srinivasan et al. [8] showed that one can use larger time steps and achieve adequate solution accuracy by using the implicit LU-SGS method by Yoon [9] along with Roe upwinding. The flux terms use a Roe upwind-biased scheme for all three coordinate directions with higher-order MUSCL-type limiting to model shocks accurately [10]. The resulting method then is third-order accurate in space and first-order accurate in time. The OVERFLOW code now has the LU-SGS method as a solver option along with 2nd order Roe upwinding.

The OVERFLOW code was designed to take full advantage of overset grid systems. Overset grid methods use a sequence of sub-grids that lie arbitrarily within a primary grid. For example, one can place a curvilinear airfoil grid within a background Cartesian grid. The airfoil grid captures detailed flow features such as the boundary layers, tip vortices, shocks, etc. The background grid surrounds the airfoil grids and carries the solution to the farfield. It is generated with some knowledge of the airfoil's surface and outer boundary point locations. Consequently, some of the background grid points lie within the airfoil's solid body regions and must be removed from the solution. Once removed, hole regions remain within the interior of the larger background grid and create a set of boundary points known as hole fringe points. The airfoil grid interpolates data to the background grid at the background's hole fringe points. Conversely, the background grid interpolates data to the airfoil grid at the airfoil outer boundary points. The solution proceeds sequentially on the individual grids with an interchange of interpolated boundary data.

Domain Connectivity Functions

With moving overset grids, individual grids move with their appropriate grid motion. As the grids move, the holes and hole boundaries change with time. To determine the grid's changing connectivity and hole points, the code known as DCF3D (Domain Connectivity Functions in Three Dimensions) by Meakin [3] was employed. DCF3D uses inverse mapping of the computational space to limit the search time and to compute hole and outer boundary interpolation stencils. The major expense in DCF3D is the creation of the inverse maps. However, the maps are independent of the relative orientation of the grids so it repeatedly uses the maps during the grid movement.

During the flowfield solution process, inter-grid boundaries are constantly changing due to the grid movement. After each flow solution time step, grid connectivity data must be redefined. After a specified number of time steps,

DCF3D is called as a subroutine within OVERFLOW to update the intergrid connectivity information and hole points

Blade Motion

The method assumes rigid blade motions in flap and pitch. The complex blade motion due to aeroelastic deformation is currently not included, however it is a straightforward modification to the method described below [11]. The periodic blade motion for pitch and flap as a function of blade azimuth, Ψ, can be described by a Fourier series [12] as shown in Equation 1 and Equation 2:

Pitch

$$\theta = \theta_o + \theta_{1c}\cos\psi + \theta_{1s}\sin\psi + \theta_{2c}\cos 2\psi + \theta_{2s}\sin 2\psi \quad (1)$$

Flap

$$\beta = \beta_o + \beta_{1c}\cos\psi + \beta_{1s}\sin\psi + \beta_{2c}\cos 2\psi + \beta_{2s}\sin 2\psi \quad (2)$$

Using only the mean and first blade harmonics, Eulerian angles prescribe the blade motion to the flowsolver. Euler parameters or Eulerian angles are useful and convenient ways to express motion of rotating bodies in terms of the fixed inertial frame.

In this method, the blade rotates about its spin axis at a given rotational rate. At each time step, the blade rotates through by an increment of $\Delta\psi$ that results in a change in pitch and flap. The incremental change in the blade position is then imposed by transforming the most current position vector to a new location through successive matrix multiplications as shown in Equation 3.

$$T = [A]\,[B]\,[C]$$
$$\vec{x}_{new} = T\vec{x}_{old} \quad (3)$$

The transformation matrix T consists of the rotation matrices A, B, and C. The matrices A,B and C represent the various coordinate rotations. See Amirouche [13] for details of the transformation matrices.

Pressure and Pressure Derivative Interpolations

The OVERFLOW code was modified to compute the pressure field and the pressure derivatives at all the gridpoints and then interpolate the resulting information onto the Kirchhoff surfaces for later postprocessing. At each point in the field the static pressure is computed from the density, mass flux and total energy as shown in Equation 4

$$P = \rho(\gamma - 1)\left[e - \frac{1}{2}\left(u^2 + v^2 + w^2\right)\right] \quad (4)$$

where P is the pressure, ρ is the density, e is the internal energy, u,v and w are the Cartesian velocities and γ is the ratio of specific heats. The temporal derivative of the pressure with respect to time, $\partial P/\partial t$, is then converted from the rotating coordinate frame to the inertial frame using the chain rule and grid metric terms as shown in Ref. [5]. The three components of the pressure gradient are also computed using the chain rule and the grid metrics from the flow solver.

At each time step, the pressure field and pressure gradient information is then interpolated to all the overset grid intergrid boundaries. To perform this interpolation, the method uses the overset grid connectivity information from the flow solver. The nonrotating Kirchhoff surfaces are then simply treated as another intergrid boundary surface that receives flow information and the pressure information.

During the flow solution process, the method stores a large quantity of data to disk for later postprocessing. At every 5 degrees of rotation, the blade geometry, flowfield conserved variables, pressure, pressure gradient and various other post processing information are stored for all of the grids. At one degree increments, the solver saves, to a separate file, the pressure information for the nonrotating Kirchhoff surfaces. The resulting Kirchhoff surfaces files are then postprocessed to compute the far-field acoustic signature.

Kirchhoff Acoustics Method

It is not practical to continue the CFD solution to large distances from the rotor blade. Large numbers of mesh points are required and the calculation rapidly becomes too large for existing computers. An alternate approach is to place a nonrotating Kirchhoff surface around the rotor blades as shown in Figure 1. A rotating-surface formulation such as that in Ref. [14,5] could also be used, however the nonrotating method avoids the problems associated with supersonic motion of the Kirchhoff surface for high-speed cases.

The Kirchhoff surface translates with the rotor hub

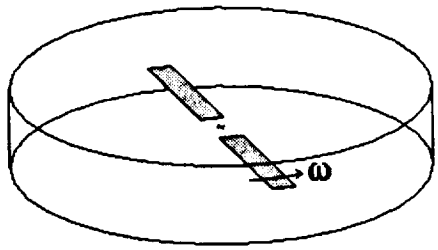

Figure 1 Nonrotating Kirchhoff surface for a helicopter rotor blade

when the helicopter is in forward flight. The acoustic pressure, p, at a fixed observer location, $\vec{x}$, and observer time, t, determined from the following integration on the cylindrical surface:

This formulation is taken from Farassat and Myers[15]. It assumes that the Kirchhoff surface is moving with Mach number $\vec{M}$. The distance between a point on the Kirchhoff surface and the observer is given by $|\vec{r}|$. Also note that the entire integral in Equation 5 is evaluated at the time of emission for the acoustic signal, τ.

$$p(\vec{x}, t) = \frac{1}{4\pi}\int_S \left\{ \frac{E_1}{|\vec{r}|(1-M_r)} + \frac{E_2 p}{r^2(1-M_r)} \right\}_\tau dS \quad (5)$$

The expressions for E_1 and E_2 are given as:

$$E_1 = \left(M_n^2 - 1\right)p_n + M_n \vec{M}_t \bullet \nabla_2 p - \left[\frac{M_n p_t}{a_\infty}\right] - \left[\frac{(\cos\theta - M_n)p_t}{a_\infty(1-M_r)}\right] \quad (6)$$

$$E_2 = \left[\frac{1-M^2}{(1-M_r)^2}\right](\cos\theta - M_n) \quad (7)$$

These expressions assume that the surface is moving with steady translational motion. Additional terms required to account for unsteady or rotational motion are given by Farassat and Myers [15].

In the above equations, M_n and M_r are the components of $\vec{M}$ normal to the Kirchhoff surface and in the direction of the observer. $\vec{M}_t$ is the velocity vector tangent to the Kirchhoff surface, and $\nabla_2 p$ is the gradient of the pressure on the Kirchhoff surface. The freestream speed of sound is assumed to be uniform at a_∞, and the angle, θ, is the angle between the normal to the Kirchhoff surface and the far-field observer.

Evaluation of the acoustic pressure at an observer time, t, requires that the integrand in Eq. (5) be evaluated at a different time of emission, τ, for each differential area element on the Kirchhoff surface. This requires two interpolations. First, the overset-grid flow solver performs a spatial interpolation of pressure and pressure derivatives directly onto the Kirchhoff surface at each time step. These interpolations use the same DCF3D connectivity program that is used with the rest the overset grids in the flow solver. The aerodynamic equations are not solved on the Kirchhoff surface mesh however. The DCF3D interpolations onto the Kirchhoff grid are very efficient and do not significantly increase the overall computational cost

After the pressure values are interpolated onto the Kirchhoff surface at each time step, they are written into a database for later use in the Kirchhoff acoustics postprocessor. For each evaluation of the integrand in Eq. (5), the appropriate value of emission time is determined by noting that the time delay between the emission of the signal and the instant that it reaches the observer is equal to the distance that the sound must travel divided by the freestream speed of sound. This formulation leads to a quadratic equation for the time of emission, τ. Further details are given in Refs. [5,6]. Once the emission time has been determined, the appropriate pressure and pressure derivative values for Eqs. (5-7) are retrieved using linear temporal interpolation in the stored CFD database.

The Kirchhoff surface consists of a top, bottom and side meshes as shown in Figure 1. Each of these meshes contains 43,200 data points for a total of 129,600 grid points. The top and bottom surfaces are located approximately 1.5 chord lengths above and below the plane of the rotor blade. The side mesh is located approximately two chords beyond the tip of the blades. The pressure data on the Kirchhoff surface is stored at intervals of one degree azimuthal angle. References [5,6] show that these Kirchhoff surface locations and temporal storage intervals are appropriate for the types of HSI and BVI noise that are modeled in this paper.

Test Cases for Aeroacoustic Simulation

HSI and BVI Cases

We have chosen two test cases for demonstration of our helicopter aeroacoustics prediction scheme. The first case simulates the high-speed impulsive (HSI) noise experiment of Schmitz et al. [16]. In this experiment, acoustic signals were recorded from a 1/7 scale model of the Army's AH-1 helicopter main rotor. The test case has a hover-tip Mach number equal to 0.665, an advance ratio of 0.258 and a rotor thrust coefficient of 0.0054. The rotor blades are rectangular and untwisted with symmetric airfoil sections and a thickness-to-chord ratio of 0.0971. The rotor blade aspect ratio is 9.22.

In spite of the fact that the HSI model rotor experiment has a significant amount of thrust, the CFD computations in this paper assume that the rotor blades are nonlifting so that the rotor wake has a minimal influence on the aerodynamics and acoustics. This approximation is not necessary since our CFD method computes the complete rotor wake system from first principles. However, we would like to directly compare our computations to those from other methods that were not able to model the rotor wake [5,6]. The justification for neglecting the rotor thrust is that HSI

pressure signals in the plane of the rotor are generally insensitive to thrust. This approximation has been experimentally documented (to first order) by Schmitz et al. [16].

Our second demonstration case is a blade vortex interaction (BVI) noise simulation that was experimentally tested by Splettstoesser et al. [17]. These experiments also used a 1/7 scale model AH-1 rotor system but the blades were twisted and pressure instrumented. Otherwise, the geometry is the same as for the HSI test described above. The aerodynamic conditions are set to a hover-tip Mach number of 0.664, an advance ratio of 0.164, and a thrust coefficient of 0.0054. The rotor tip-path plane is tilted back by one degree in order to cause blade-vortex interactions and the rotor has 0.5° of precone. This combination produces a both advancing and retreating-side BVI's plus advancing side unsteady transonic flow. Accurate numerical resolution of the rotor wake system is very important for the numerical resolution in this test case since the tip vortices have a strong influence on the unsteady aerodynamics and acoustics.

OLS Blade Grid System

The aeroacoustic overset grid system for the OLS rotor consists of 14 overset grids as highlighted in Figure 2a. Eight of the grids were generated primarily to capture the aerodynamic flow field as shown in Figure 2b. These grids consist of one for each rotor blade, one for each blade tip, and one transition grid to help connect the blade grids the single global background grid. The rotor grid is of C-H topology with clustering near the tip, root and leading and trailing edges. A tip-cap grid captures the shape of the blade and also allows for more accurate prediction of tip vortex formation. At the inboard sections, the blade grids collape to a slit singularity. The hyperbolic grid generator by Chan, et. al [18] generated the resulting blade volume grids illustrated in Figure 2b.

The blade grids lie within a Cartesian intermediate grid with points concentrated in the vicinity of the blade. The intermediate grid extends approximately 3 rotor chords beyond the rotor blade tips, above and below the rotor plane. The global background grid completes the overset grid system. The global grid extends to 4 blade radii from the hub center upstream, downstream and to the sides. The grid also extends 2 blade radii above the blade and 2.5 radii below.

The function of the remaining grids is to accurately compute the pressure information required for the Kirchhoff integration. An additional CFD grid is overset in the vicinity of the blade tip and extends to just beyond the surrounding nonrotating Kirchhoff surfaces, Figure 2c. This grid has a simple H-H topology. It is smoothly clustered with fine resolution that follows the linear characteristics of the acoustic waves. This minimizes dissipation in the propagating acoustic signals. Finally, the Kirchhoff surface surrounds the entire blade and tip extension grids at an appropriate distance as described earlier

The entire moving overset system totals roughly 1.47 million grid points. During the grid motions, the background grid remains stationary as the rotor blade and intermediate grids rotate through the stationary grid. As the blade grids rotate about the spin axis, they pitch and flap accordingly. During their pitch and flap motions, the blade grids create holes within the intermediate grids while the intermediate grid creates holes within the background grid. The Kirchhoff surface grids then interpolate information based on a chosen preference list. In descending this list is: 1) tip extension grid, 2) tip cap grid, 3) blade and then finally 4) intermediate.

Computer Implementation for the Two Test Cases

Both the HSI and BVI test cases use the same grid system that was described earlier. This means that both simulations require the same amount of computer resources for each time step of the flow solver. Note that the background grid is very coarse, with uniform spacings of approximately 0.25 blade chord lengths. This grid is too coarse to accurately convect the rotor wake system, so we do not expect to see good results for the BVI noise.

With this grid system (1.47 million total mesh points), the OVERFLOW code requires 32.0 seconds per time step on one processor of the Cray C-90. The time-accurate calculation impulsively starts from freestream conditions with the viscous no-slip boundary condition applied at the blade surfaces. The HSI noise case requires one half revolution to eliminate the transient effects from this impulsive start. Afterwards, the complete solution can be computed in an additional one half revolution and stored for later postprocessing of the aerodynamic and the acoustic data. As mentioned before, the interpolation of pressure data onto the Kirchhoff surface does not significantly increase the total computation time. With a typical time step of 0.25 degrees of azimuthal angle, the total time for this calculation is 13 Cray C-90 hours.

The BVI noise computation requires two and a half revolutions blade revolutions to eliminate the transient starting conditions. This longer start-up period is a result of additional unsteadiness of the rotor wake system which was not a factor in the HSI case. With a typical time step of 0.25 degrees of azimuthal angle, the total time for this calculation is about 38 Cray C-90 hours.

One aspect of these unsteady rotor calculations is that they produce a very large amount of output data. Our calculations store the complete solution for all 1.47 million

grid points at 5 degree azimuthal intervals. The solution for pressure and pressure gradients on the Kirchhoff surface is stored at one degree intervals. Additional postprocessing information for force and moment and surface pressures are also stored at 5 degree intervals. Because these files are so large, they must be moved onto an auxiliary storage device after each half revolution. The total amount of stored data per rotor revolution is approximately 15GBytes.

Once these files are moved to auxiliary storage, they later retrieved for visualization and acoustics postprocessing. Visualization of these large datasets requires a dedicated Convex computer system that is part of the Time-Accurate Visualization System (TAVS) at NASA Ames Research Center. The pressure data required by the Kirchhoff integration is retrieved to the Cray C-90 where it is split into six different pieces for the Kirchhoff program. The Kirchhoff integration computes the acoustic pressure contributions separately from each piece of the surface in order to reduce the total in-core memory requirements. These pressure contributions are later summed to determine the total far-field observer pressures.

The Kirchhoff integration program requires 0.075 CPU seconds for each evaluation of pressure in Eq. (5) at an observer location in space, and an observer time, t. The Kirchhoff program runs at 470 MFLOPS on the Cray C-90 and the overall speed is approximately 20 times faster than the CPU times reported in Ref. [5]. The reason for this speedup is that the spatial interpolations onto the Kirchhoff surface are now computed by the flow solver, and not by the Kirchhoff integration program. The elimination of these interpolations allows the code to run much faster on the C-90. The in-core memory requirement for the Kirchhoff code is 19MW. This cost could be further reduced by splitting the Kirchhoff surface up into smaller pieces.

Results: High-Speed Impulsive Noise

Computed results for the HSI case are compared in Figure 3 to the experimental data for several different far-field microphones. The microphone numbers in this figure correspond to those used in Refs. [16,17]. Also shown in this figure are computed results from the TURNS/Kirchhoff analysis in Ref. [5]. The current calculations show good agreement with the data in the signal width and phase for all of the microphones. The peak negative pressures are underpredicted for microphones 1,2 and 6 however. The TURNS/Kirchhoff predictions have higher amplitudes and show better agreement with the data.

The reason for the differences between the two CFD/Kirchhoff predictions in Figure 3 can be explained with the help of Figure 4. Here, the computed chordwise pressure coefficient at 90° azimuthal angle and 0.95 rotor span is plotted from the current Navier-Stokes calculation and from the TURNS Euler equation solution in Ref. [5]. The TURNS solution shows a much sharper shock and this leads to far-field acoustic signals with larger peak negative pressures.

There are two reasons why the TURNS calculation has a stronger shock at 90° azimuthal angle. First, the TURNS code was run in the inviscid Euler mode while the current OVERFLOW calculations solve the viscous Navier-Stokes equations. The addition of viscosity tends to weaken the shock on the advancing side of the rotor blade. Also, the TURNS code uses a third-order accurate spatial differences scheme while the current OVERFLOW code uses a second order scheme. The lower-order OVERFLOW scheme tends to smear the shock more and this results in a lower peak negative pressure in the far-field acoustics. Improvement of the spatial difference scheme in OVERFLOW is a high priority for future calculations.

One interesting observation on the computed OVERFLOW results in Figure 3 is that they were run with a time step of 1/16 of a degree azimuthal angle. We originally ran this case with a time step of 1/4 degree, but obtained poor results, particularly in the second quadrant of blade motion where unsteady transonic effects are high. A time step of 1/16 degree was ultimately required for time accuracy.

Results from the TURNS code in Ref. [5] used time steps of 1/4 degree with good results. This was initially surprising because TURNS code uses the same LU-SGS implicit solver that is used in OVERFLOW. The difference is that the TURNS computations used 3 "Newton" subiterations per time step in order to reduce the factorization error in the LU-SGS algorithm. The implementation of the Newton subiterations is explained in Ref. [8]. Currently, there is no option for Newton subiterations in the OVERFLOW code and our time accuracy suffered accordingly. Programming of the Newton scheme in the LU-SGS algorithm is an important priority for future OVERFLOW calculations.

Figure 5 illustrates the effect of time step changes on the acoustics solution at microphone 8. Reduction of the time step to 1/16 degree azimuthal angle has a dramatic effect on the accuracy of the calculation. The reason why microphone 8 is so sensitive to time step changes is explained with reference to Figure 6. The line contours on this figure show the contributions from the Kirchhoff surface to the peak negative pressure value at microphone 8. These contour lines correspond to a different time of emission, τ, for each signal on the Kirchhoff surface that reaches microphone 8 at a single observer time.

These Kirchhoff-surface contours show that the peak pressure signal that reaches microphone 8 corresponds to noise that was emitted from the Kirchhoff surface when the advancing-side rotor blade was near 135° azimuthal

angle. Thus, the peak acoustic pressure signal for microphone 8 is produced when the rotor blade is in the second quadrant of motion, which is exactly where the transonic unsteadiness is highest in the CFD solution. If the unsteady time step is too large in the CFD solution, we should expect the maximum temporal errors to occur in the second quadrant of blade motion and the maximum errors in far-field acoustics to occur near microphone 8, which is what we see in practice.

The acoustic contributions to microphones 1, 2, and 8 come from a region on the Kirchhoff surface where the blade is near 90° azimuthal angle. The unsteady transonic effects are not as important here and we expect the solution to be less sensitive to changes in time step. This is also exactly what we see in practice.

Results: Blade-Vortex Interaction Noise

The BVI case was computed with a time step of 1/4 degree azimuthal angle. Our HSI calculations have demonstrated that this is inadequate when there are transonic unsteady effects in the second quadrant of blade motion. In addition to these time-accuracy problems, our background grid is too coarse to numerically resolve the tip vortices in the rotor wake.

In spite of these known problems, we present results for the BVI noise test case. Even though the computed results are somewhat inaccurate, they demonstrate the capabilities and potential of the overall scheme for computing general BVI noise.

Figure 7 compares computed and experimental results for chordwise pressure coefficient at 0.975 rotor span. Experimental pressures are only available for a limited number of upper-surface locations on the advancing side of the rotor disk. The computed results show good agreement with the experimental data in the first quadrant of rotor motion. There is a significant discrepancy at 135 degrees azimuthal angle however, and this is most likely due to time-accuracy problems associated with the 1/4 degree time steps. The remedy for this problem is either to use a smaller time step as in the HSI case, or to implement the "Newton" subiterations in the LU-SGS scheme that are described in Ref. [8].

Figure 8 compares computed and experimental differential pressures near the leading edge at 0.91 rotor span. The computed differential pressures are too high in the first quadrant, but show an indication of the blade-vortex interaction that occurs near 90°. The computed pressures are much too high in the second quadrant, which is another indication of temporal inaccuracy in this region. Finally, the computation completely misses the strong blade-vortex interaction near 270° azimuthal angle. This is most likely due to the fact that the far-field grid is much too coarse to resolve the tip vortices in the rotor wake without excessive dissipation.

On the brighter side, the computed thrust value, C_t, is equal to 0.0053, which is very close to the experimental value of 0.0054. In addition, the computed roll moments are very close to zero which indicates that the use of experimental settings for the blade motion produce a trimmed solution in the computation.

Figure 9 compares far-field acoustics predictions with the experimental measurements at microphone 3. This microphone is located directly in front of the rotor disk and 30° below the plane of the rotor.

Because of the known problems in the aerodynamic solution, it is not surprising that the Kirchhoff integration produces poor agreement with the experimental data. Improvements in the aerodynamic solution should result in better far-field acoustics results.

Summary and Conclusions

This paper presents an overall framework to compute helicopter aerodynamics and acoustics. The key elements in this framework are the overset grid generation, the domain connectivity control (DCF3D), the Navier-Stokes flow solver (OVERFLOW), and the Kirchhoff acoustics integration. One way that this analysis differs from earlier work is that the rotor wake system is computed as an inherent component of the total flowfield. Once we specify the blade motions, the wake and surface aerodynamics are computed in a tightly-coupled manner. In addition, interpolation onto the nonrotating Kirchhoff surface is performed by the flow solver at a negligible additional cost. Finally, the overset-grid scheme offers a framework for including finite-element models for blade dynamics as discussed in Ref. [11].

Because the overall analysis has several key components, all of these must be functioning accurately in order to produce accurate far-field noise simulations. Results from the two test cases show that three weak spots exist in the analysis package. The first is time-accuracy in the flow solver. This will be addressed by adding Newton subiterations at each unsteady time step to the LU-SGS solution algorithm. This has worked well in the TURNS code [8] and should also be successful in OVERFLOW.

The second weak spot is the spatial difference scheme in OVERFLOW. Higher order spatial accuracy will reduce numerical dissipation and help preserve the vortex structures and shock waves on the rotor surface. A final improvement for BVI noise prediction requires the use of solution-adaptive grids in order to minimize numerical dissipation in the rotor wake. This deficiency is being addressed with overset-grid compatible schemes such as

the those proposed in Ref. [2,19,20].

In spite of the limitations discussed above, the methodology in this paper offers the potential for major improvements in our aeroacoustic prediction capability. Earlier methods based on comprehensive codes, lifting-line aerodynamics and the acoustic analogy have matured to a point where future fundamental improvements to the methods are unlikely. The main problem in these methods is the accurate simulation of the rotor wake system.

We don't claim to have solved the rotor wake problem yet, but our CFD-based aeroacoustics scheme offers a clear path to maximize the payoff from future improvements in CFD rotor-wake modeling. Any such improvements should immediately enhance our ability to model helicopter rotor noise.

References

[1]Ahmad, J.U., and Duque, E.P.N., "Helicopter Rotor Blade Computation in Unsteady Flows Using Moving Embedded Grids", AIAA Paper 94-1922, July 1994.

[2]Duque, E. P. N., Biswas, R., and Strawn, R. C., "A Solution-Adaptive Structured/Unstructured Overset Grid Flow Solver with Applications to Helicopter Rotor Flows," AIAA-95-1766, 13th AIAA Applied Aerodynamics Conf., San Diego, CA, June 19-21, 1995.

[3]Meakin, R., "Moving Body Overset Grid Methods for Complete Aircraft Tiltrotor Simulations," AIAA Paper 93-3350, 11th AIAA Computational Fluid Dynamics Conference, July 1993, Orlando, Florida.

[4]Duque, E. P. N., and Srinivasan, G. R., "Numerical Simulation of a Hovering Rotor Using Embedded Grids," Proceedings of the 48th AHS Annual Forum and Technology Display, Washington, DC, June 3-5, 1992.

[5]Strawn, R. C., Biswas, R., and Lyrintzis, A.S., "Helicopter Noise Predictions using Kirchhoff Methods", 51st Annual Forum of the American Helicopter Society, Fort Worth, TX, May 1995 (to appear in J. of Comp. Acoustics).

[6]Strawn, R. C., and Biswas, R., ``Computation of Helicopter Rotor Acoustics in Forward Flight," Journal of the American Helicopter Society, Vol. 4, No. 3, July, 1995, pp. 66--72.

[7]Buning, P., Chan, Rieze, and Sondak, *OVERFLOW 1.6ap Users Manual*, Feb 1995.

[8]Srinivasan, G. R., Baeder, J. D., Obayashi, S., and McCroskey, W.J.,"Flowfield of a Lifting Rotor in Hover: Navier-Stokes Simulation," *AIAA Journal*, Vol. 30, No. 10, Oct. 1992, pp 2371-2378.

[9]Yoon, S. and Jameson, A., "An LU-SSOR Scheme for the Euler and Navier-Stokes Equations," AIAA Paper 87-0600, Jan, 1987.

[10]van Leer, B., Thomas, J.L., Roe, P.L. and Newsome, R.W., "A Comparison of Numerical Flux Formulas for the Euler and Navier-Stokes Equations," AIAA Paper 87-1104, June 1987.

[11]Ahmad, J.U. , Bauchau O. and Duque, E.P.N., "Aeroelastic Prediction of a Helicopter Rotor in Forward Flight", Sixth International Symposium on Computational Fluid Dynamics, September 1995

[12]Johnson, W, *Helicopter Theory*, Princeton University Press, 1980.

[13]Amirouche, F.M.L., *Computational Methods in Multibody Dynamics*, Prentice Hall, 1992.

[14]Xue, Y., and Lyrintzis, A.S., "Rotating Kirchhoff Method for Three-Dimensional Transonic Blade Vortex Interaction Hover Noise," *AIAA Journal*, Vol. 32, No. 7, Jul. 1994, pp.1350-1359.

[15]Farassat, F., and Myers, M. K., "Extension of Kirchhoff's Formula to Radiation from Moving Surfaces," Journal of Sound and Vibration, Vol. 123, No. 3, 1988, pp. 451-460.

[16]Schmitz, F. H., Boxwell, D. A., Splettstoesser, W. R., and Schultz, K. J., "Model-Rotor High-Speed Impulsive Noise: Full-Scale Comparisons and Parametric Variations," Vertica, Vol. 8, No. 4, 1984, pp. 395-422.

[17]Splettstoesser, W. R., Schultz, K. J., Boxwell, D. A., and Schmitz, F. H., "Helicopter Model Rotor-Blade Vortex Interaction Impulsive Noise: Scalability and Parametric Variations" presented at the 10th European Rotorcraft Forum, The Hague, Netherlands, Aug. 28-31, 1984.

[18]Chan, W.M., Chiu, I.T., and Buning. P.G., "User's Manual for the Hyperbolic Grid Generator and the HGUI Graphical User Interface," NASA TM 108791, October 1993.

[19]Meakin, R., L., "An Efficient Means of Adaptive Refinement Within Systems of Overset Grids," AIAA-95-1722, presented at the 12th AIAA Comp. Fluid Dynamics Conf., San Diego, CA, June 19-22, 1995.

[20]Ramachandran, K., Tung, C., and Caradonna, F. X., "Rotor Hover Performance Prediction Using a Free Wake CFD Method," Journal of Aircraft, Vol. 26, No. 12, December 1989, pp. 1105-1110.

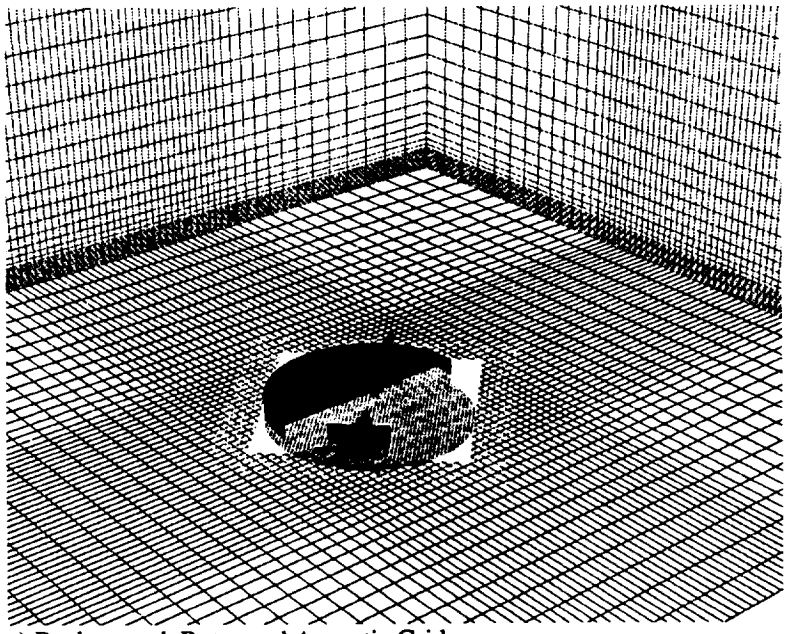

a) Background, Rotor and Acoustic Grids

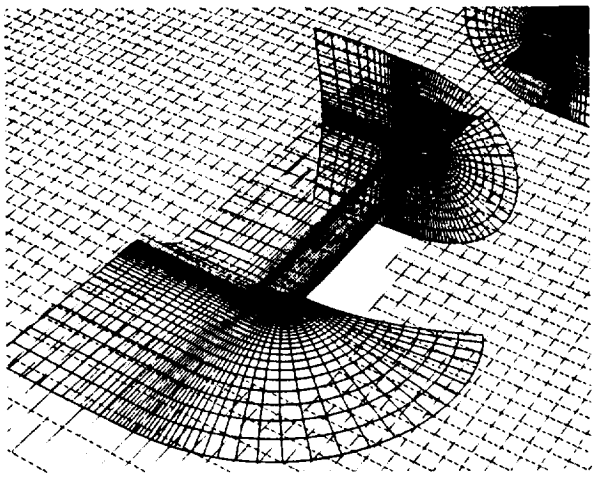

b) Blade, Tip Cap and Intermediate Grids

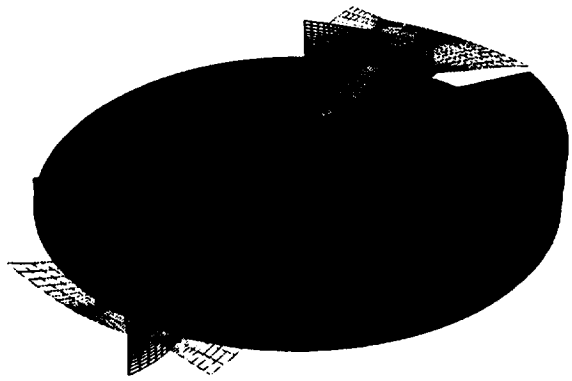

c) Kirchoff Surfaces and Tip Extension

Figure 2 Aerodynamic and Acoustic Overset Grid System for OLS Rotor

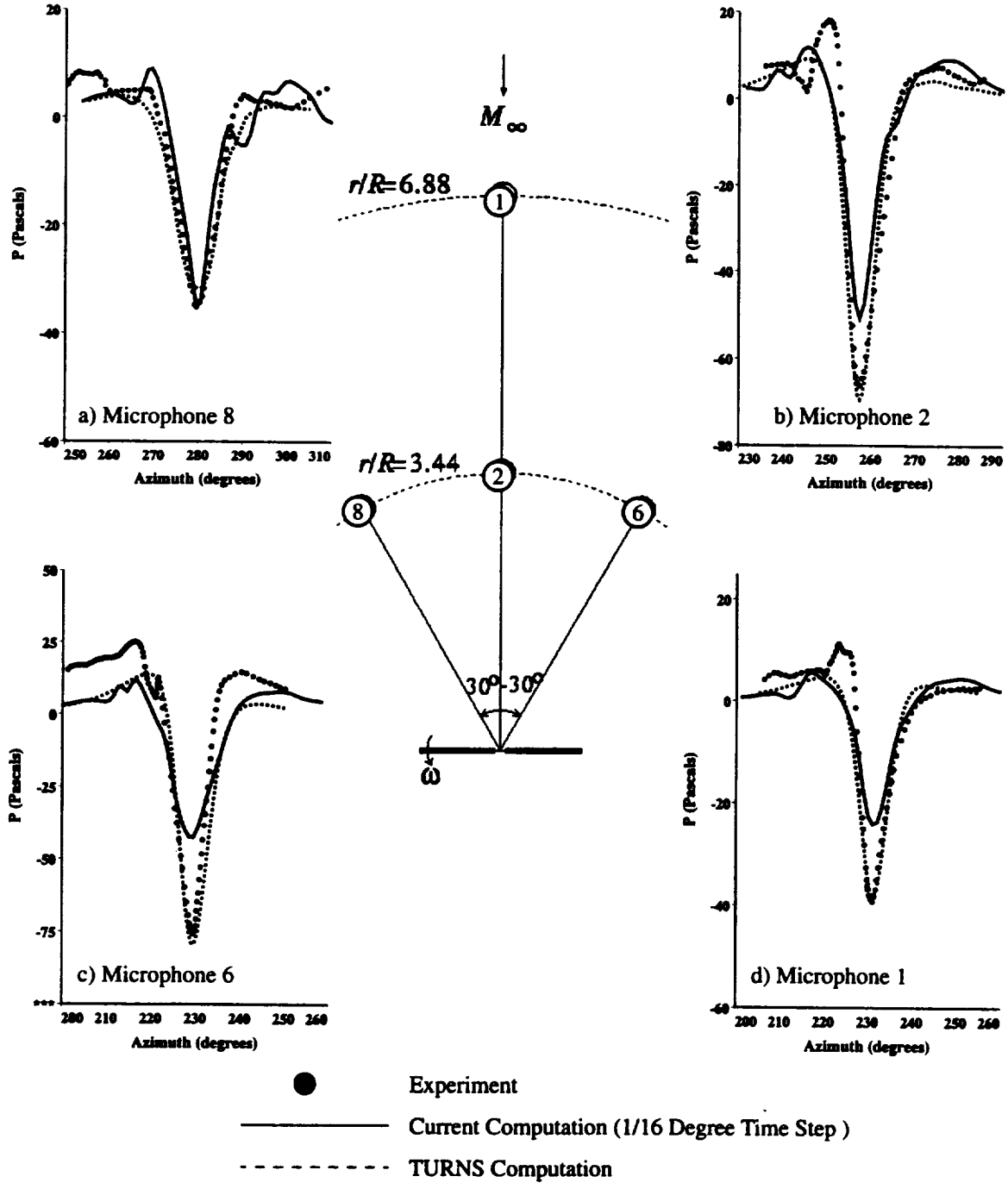

Figure 3 OLS, HSI Case, dt= 1/16 Degree per time step
M_t= 0.665, μ=0.258

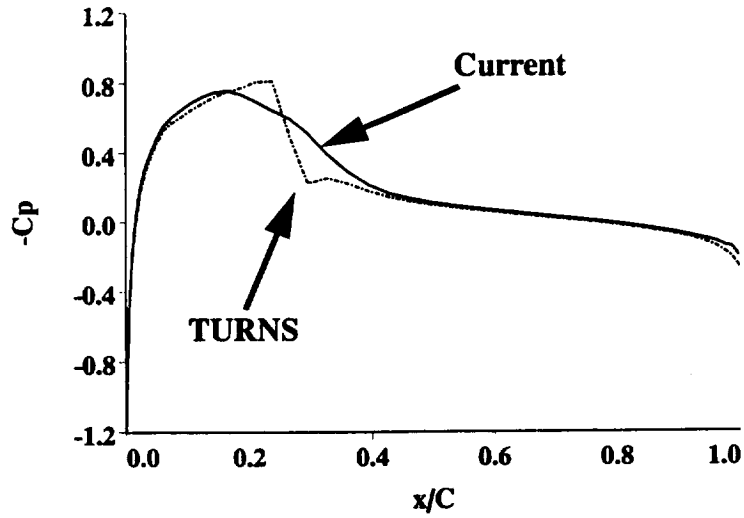

Figure 4 Pressure Coefficient Comparison between TURNS and current
Ψ=90°, r/R = 0.95
HSI Case M_t= 0.665, μ=0.258

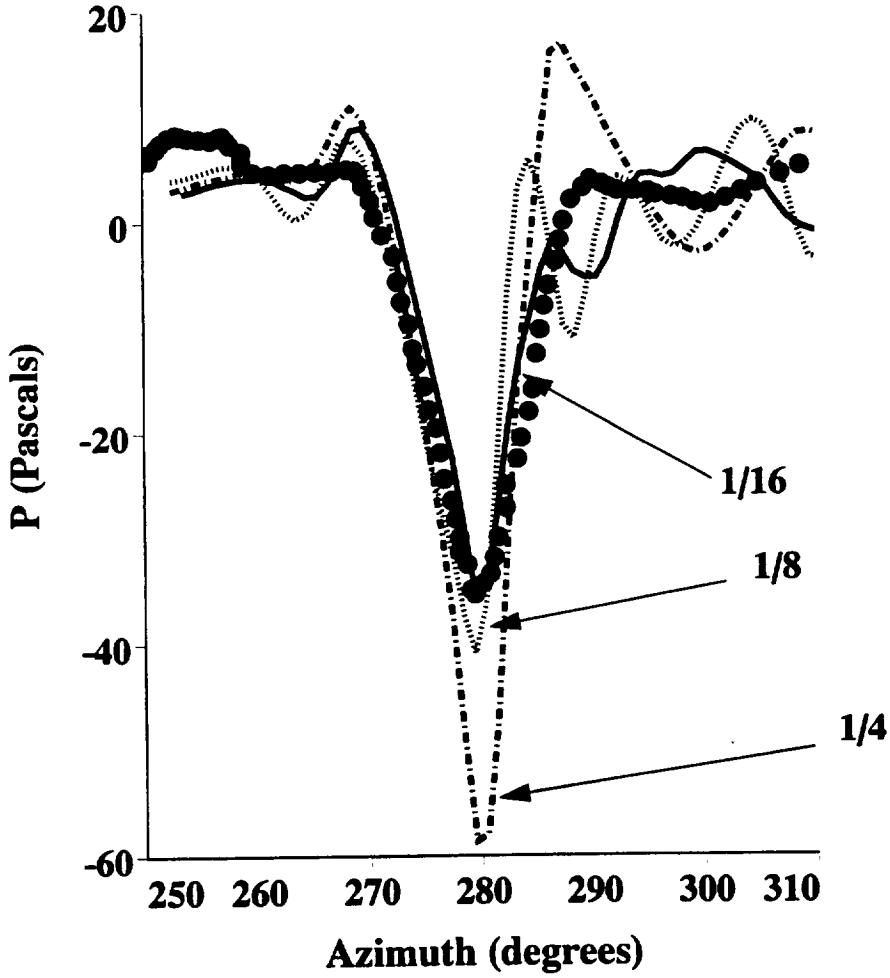

Figure 5 Microphone 8, HSI Case, dt= 1/4, 1/8 1/16 Degree per time step
M_t= 0.665, μ=0.258

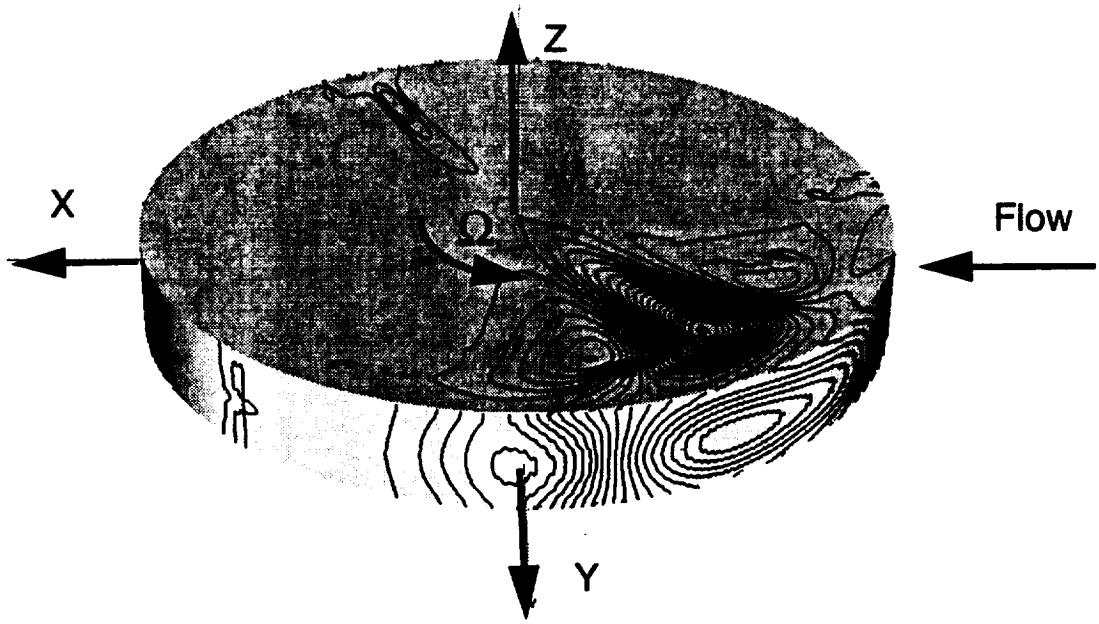

Figure 6 Kirchhoff Surface Contributions to Peak Pressure at Microphone 6
HSI Case, M_t= 0.665, μ=0.258

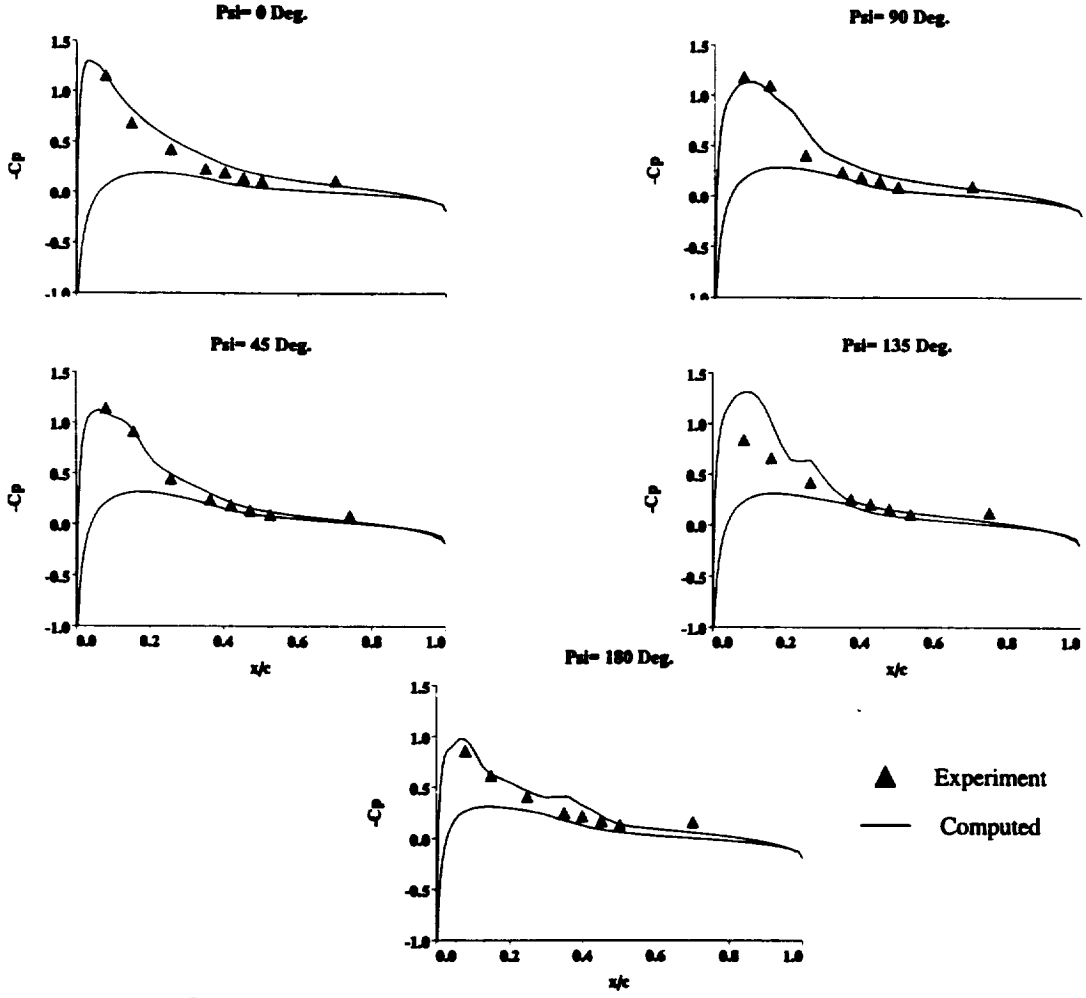

Figure 7 OLS Chordwise Surface Pressure Distributions (run 10014)
BVI Case, μ=0.164, M_t=0.664, C_t=0.0054

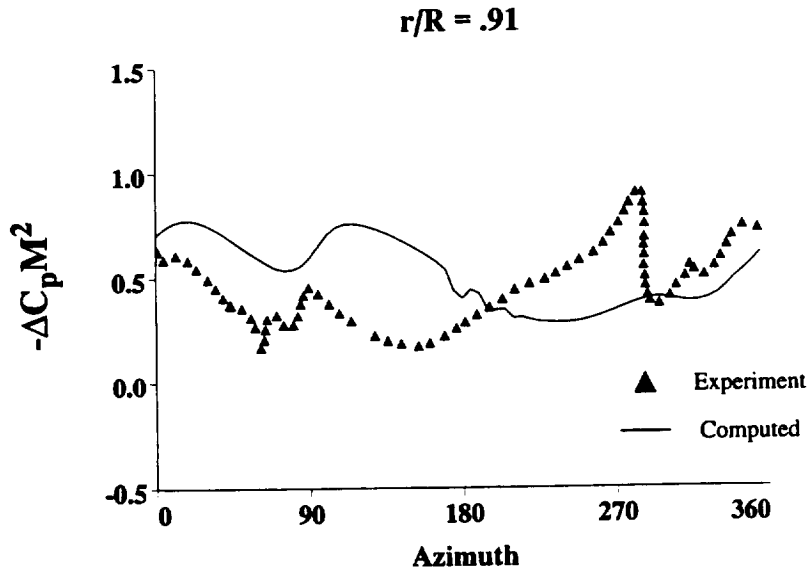

Figure 8 OLS Chordwise Differential Pressures x/c=0.03 (run 10014)
μ=0.164, M_t=0.664, C_t=0.0054

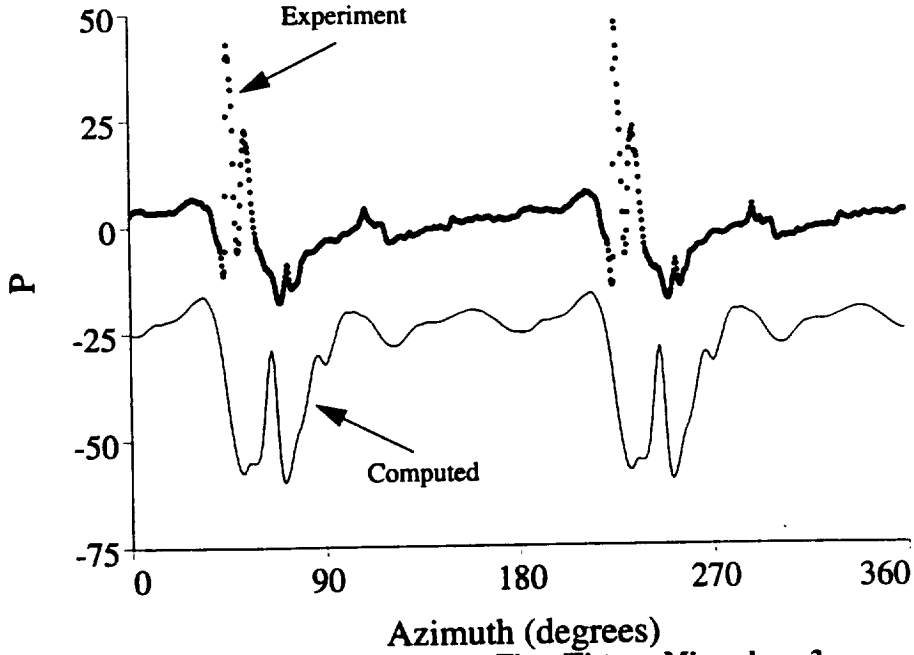

Figure 9 Farfield Microphone Time History, Microphone 3
μ=0.164, M_t=0.664, C_t=0.0054

RIACS
Mail Stop T041-5
NASA Ames Research Center
Moffett Field, CA 94035